EFFECT OF SPECIMEN THICKNESS ON CRACK FRONT PLASTICITY CHARACTERISTICS IN THREE-DIMENSIONS

E. Moyer, Jr. and H. Liebowitz

School of Engineering and Applied Science, The George Washington University, Washington, D.C., USA

ABSTRACT

A finite element investigation of the effect of thickness on plastic deformation and yielding characteristics in three-dimensional cracked bodies is presented. It is shown that the fundamental deformation modes and extent of plastic deformation are significantly influenced by the specimen thickness. The results show the transition from a local plane strain to plane stress response near the crack front as the specimen thickness is decreased. While the results are generated for a specific aluminum alloy (7075-T7651), the predictions for other hardening materials would be qualitatively the same.

KEYWORDS

Nonlinear finite-element calculations, plastic deformation, three-dimensional crack specimens, incremental analysis.

INTRODUCTION

Of fundamental importance to the accurate fracture assessment of components and structures made of metals is the study of ductile fracture processes and the plastic response near a crack. The basic deformation response near the crack front must be resolved accurately for reliable predictions. Fracture criteria have been proposed based on many controlling quantities (e.g., stress, strain, energy, displacements, etc.) both on global and local scale levels. Without exception, all of these criteria require accurate local deformation modeling.

To understand the scale shifting effects from the laboratory specimen to the structural component, it is imperative to discover the effects of specimen thickness on the deformation response. This problem is an essentially three-dimensional one and must be investigated accordingly.

The purpose of this investigation is to delineate the effect of specimen thickness on local crack front yielding characteristics in a cracked specimen. The three-dimensional elastic plastic finite element code developed in [1] is employed for the analysis. Specimen thicknesses investigated range

from well beyond ASTM plane-strain requirements to thin sheet dimensions. The yield zones calculated in this work demonstrate the transition from dilatational to distortional dominance ahead of the crack tip as a function of thickness (equivalent to a transition from plane strain to plane stress). The magnitude as well as the extent of yielding is shown to be highly thickness dependent. The results of this study also demonstrate that two-dimensional analysis based on plane strain (for thick specimens) or plane stress (for thin specimens) can fail to accurately model the local response when simple standards would dictate otherwise.

PLASTICITY FORMULATION

The incremental theory of plasticity employed in this work is based on the classical rate proportionality assumptions and J_2 flow theory. While the mathematical details vary with the choice of yield criteria, the salient features of all incremental theories are the same. This discussion will, therefore, be confined to the specific theory employed in this work.

Assuming stress strain rate proportionality and J_2 flow theory (which assumes the plastic deformations are incompressible) the stress-strain rate relations can be written as [2]

$$\dot{e}_{ij} = \begin{cases} \frac{1+\nu}{E}\dot{S}_{ij} + \frac{3}{2} f(\sigma_e) S'_{ij}\dot{\sigma}_e & \sigma_e = \sigma_y;\ \dot{\sigma}_e > 0 \\ \frac{1+\nu}{E}\dot{S}_{ij} & \text{Otherwise} \end{cases} \tag{1}$$

where:

$\dot{e}_{ij} = \dot{\varepsilon}_{ij} - \frac{1}{3}\dot{\varepsilon}_{pp}\delta_{ij}$ are the deviatoric strain rate components,
ν is Poisson's ratio,
E is Young's modulus,
$S_{ij} = \sigma_{ij} - \frac{1}{3}\sigma_{pp}\delta_{ij}$ are the deviatoric stress components,
a_{ij} are the coordinates in stress space of the yield surface center
$S'_{ij} = S_{ij} - a_{ij}$ are the deviatoric stress components measured relative to the current yield center,
$\sigma_e = \sqrt{\frac{3}{2} S_{ij}S_{ij}}$ is the effective stress,
$\sigma'_e = \sqrt{\frac{3}{2} S'_{ij}S'_{ij}}$ is the effective stress relative to the current yield center,
σ_y is the current yield stress, and
$\cdot$ denotes time differentiation.

Due to the plastic incompressibility condition, the hydrostatic strain rate is proportional to the mean stress rate and is given by

$$\dot{\varepsilon}_{pp} = \frac{1-2\nu}{E}\dot{\sigma}_{pp} \tag{2}$$

The function $f(\sigma_e)$ is dependent on the uniaxial stress-strain curve and will be discussed subsequently. For a von Mises (J_2) material, the center of the yield surface moves at a rate proportional to the projection of the stress rate vector onto the local normal to the current yield surface and can be written as

$$a_{ij} = \begin{cases} \frac{3}{2}(1-\beta) S'_{k\ell}\dot{S}_{k\ell}S'_{ij}/\sigma'^{2}_e & \sigma_e = \sigma_y;\ \dot{\sigma}_e > 0 \\ 0 & \text{Otherwise} \end{cases} \tag{3}$$

where β varying from 0 to 1 will model hardening behavior from kinematic ($\beta = 0$) to isotropic ($\beta = 1$).

The function $f(\sigma_e)$ is derived from the uniaxial stress-strain curve. For a uniaxial specimen, equation (1) reduces to

$$\frac{2}{3}(\dot{\varepsilon}_{axial} - \dot{\varepsilon}_{transverse}) = \frac{2}{3}\left(\frac{1+\nu}{E}\right)\dot{\sigma}_e + f(\sigma_e)\,\sigma_e\dot{\sigma}_e \tag{4}$$

Thus, in the plastic range

$$f(\sigma_e) = \frac{2}{3}(\dot{\varepsilon}_{axial} - \dot{\varepsilon}_{transverse})/\sigma_e\dot{\sigma}_e \tag{5}$$

Invoking incompressibility (i.e., $\dot{\varepsilon}_{transverse} = -\frac{1}{2}\dot{\varepsilon}_{axial}$), the function $f(\sigma_e)$ can be written as

$$f(\sigma_e) = \dot{\varepsilon}_{plastic}/\sigma_e\dot{\sigma}_e \tag{6}$$

If the uniaxial stress-strain curve is expressed in a multilinear fashion, the stress-strain relation is

$$\varepsilon = \frac{\sigma}{E} + \frac{\alpha_1}{E}(\sigma_1-\sigma_y) + \frac{\alpha_2}{E}(\sigma_2-\sigma_y) + \ldots + \frac{\alpha_m}{E}(\sigma-\sigma_m) \tag{7}$$

where $\sigma_{m-1} < \sigma < \sigma_m$ and α_m is given by

$$\alpha_m = \frac{E\Delta\varepsilon_m - \Delta\sigma_m}{\Delta\sigma_m} \tag{8}$$

From equation (7), the plastic strain rate is given by

$$\dot{\varepsilon}_{plastic} = \frac{\alpha_m\dot{\sigma}_e}{E} \tag{9}$$

and thus from (6)

$$f(\sigma_e) = \frac{\alpha_m}{E\sigma_e} \tag{10}$$

Equations (1), (2), (3) and (10) provide a complete set of elastic-plastic constitutive relations. Together with the equilibrium equations and the strain-displacement relations, a governing system will be formed. It is important to note that the constitutive formulation outlined above is acceptable for finite as well as infinitesimal strains. Also of importance is the fact that this formulation is strain-rate independent. This assumption appears to be realistic for most engineering metals at room temperature (or cooler). For high temperature problems a rate-independent formulation is dubious.

Equations (1), (2), (3) and (10) provide the fundamental relationships between stress and strain rates. The equilibrium conditions (governing equations) for a continuum body in the absence of body forces and inertia effects can be written as

$$\partial \dot{\sigma}_{ij}/\partial x_j = 0 \tag{11}$$

with the boundary conditions

$$\dot{\sigma}_{ij} n_j = \dot{T}_i \text{ on } S_T$$

and

$$\dot{u}_i = \dot{\hat{u}}_i \text{ on } S_u \tag{12}$$

where $\dot{T}$ are the specified loading rates on the boundary experiencing applied tractions (S_T) and $\dot{\hat{u}}_i$ are the velocities specified on the remainder of the boundary (S_u). Utilizing the standard infinitesimal strain-displacement relations

$$\dot{\varepsilon}_{ij} = \frac{1}{2}(\partial \dot{u}_i/\partial x_j + \partial \dot{u}_j/\partial x_i) \tag{13}$$

and either employing the Principle of Virtual Work for increments of displacement or by performing the standard Galerkin technique on the governing equations, (11) and (12), the finite element equations governing the nodal velocities, $\dot{U}$ can be written in terms of the loading rate vector, $\dot{R}$, in the form

$$\underset{\sim}{K}(\underset{\sim}{U}) \cdot \dot{\underset{\sim}{U}} - \dot{\underset{\sim}{R}} = 0 \tag{14}$$

The standard finite element assumptions made are given by

$$\begin{aligned} \underset{\sim}{u} &= \underset{\sim}{N} \cdot \underset{\sim}{U} \\ \dot{\underset{\sim}{\varepsilon}} &= \underset{\sim}{B} \cdot \dot{\underset{\sim}{U}} \\ \dot{\underset{\sim}{\sigma}} &= \underset{\sim}{D}(\underset{\sim}{U}) \cdot \dot{\underset{\sim}{\varepsilon}} \end{aligned} \tag{15}$$

$$\underset{\sim}{K}(\underset{\sim}{U}) = \sum_{\text{elements}} \int_{\text{element volume}} \underset{\sim}{B}^T \underset{\sim}{D}(\underset{\sim}{U}) \underset{\sim}{B} \, dA$$

where N are the shape functions. The set of rate equations (14) will be integrated one load increment (ΔR) at a given time to determine the corresponding new displacement increment, ΔU. The Newton-Raphson or tangent stiffness solution procedure is employed as described in [3].

PROBLEM DESCRIPTION

To study the effects of specimen thickness on the yielding characteristics of typical fracture specimens, a finite center-cracked plate was chosen for investigation. The standard mode I configuration shown in Fig. 1 was analyzed for total thicknesses of

2T = 2.54 cm 2T = 1.27 cm
2T = 6.35 mm 2T = 3.175 mm

The material investigated was a 7075-T7651 aluminum alloy with elastic properties

$E = 7.24$ E+04 MPa

$\nu = 0.3$

$\sigma_y = 4.07$ E+02 MPa

The uniaxial stress-strain curve is shown in Fig. 2.

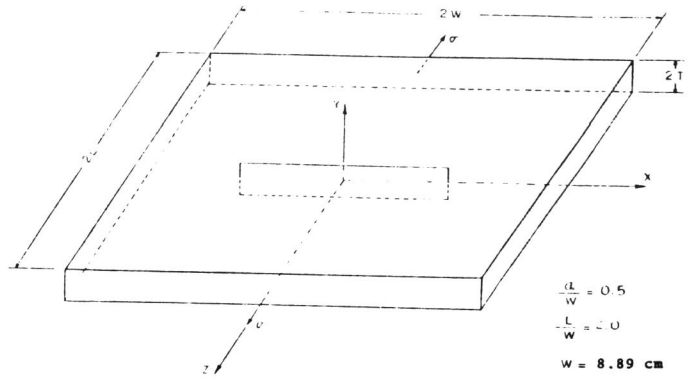

Fig. 1. Through crack geometry and loading.

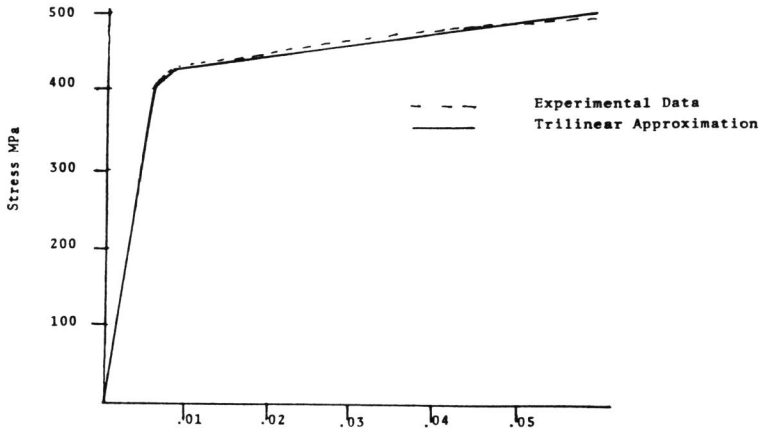

Fig. 2. Uniaxial stress-strain curve for 7075-T6751 aluminum.

The finite element discretization employed in the analysis utilizes 20-Node quadratic isoparametric elements exclusively. A fine mesh near the crack front is employed for accurate modeling. The grid characteristics and convergence properties are discussed in [1,4]. The maximum load applied was

$\sigma_{max} = 1.77$ E+02 MPa

A hardening parameter of $\beta = 0.5$ was also assumed in the analysis.

RESULTS AND DISCUSSION

The yield zones predicted at the maximum load for each of the four thicknesses studied were calculated and plotted both on the surface and midplane of the specimen. The results demonstrate the significant influence thickness has both on the nature and extent of the yielding.

Figure 3a is a plot of the von Mises stress contour corresponding to the specimen yield stress calculated at the maximum load on the surface of the 2.54 cm thick specimen. As expected for a thick specimen, this zone has the characteristic form of a plane strain yield zone (i.e., minimal yielding ahead of the crack tip and a very upright yield zone). The maximum extent of yielding is 30.7% of the half crack length which is consistent with the small strain assumptions made in the analysis requiring contained yielding. Figure 3b is a plot of the surface zones for a specimen with total thickness of 1.27 cm. The yield zone is slightly wider (more rounded) with this thickness. The maximum radius is now 32.7% of the half crack length and the yielding ahead of the tip has increased (though it is still small). The zone still maintains the basic plane strain characteristics at this thickness.

Figure 3c shows the surface yield zone for a specimen with thickness of 6.35 mm. The zone is now much wider with a larger maximum radius and yield extent ahead of the tip. The zone no longer exhibits the plane strain characteristics but is in transition between plane strain and plane stress. Figure 3d is a plot of the surface yield zone for a specimen with total thickness of 3.175 mm. The zone is significantly more rounded than any of the previous zones with a larger maximum radius and yield extent. The maximum yield radii and extent of yielding ahead of the crack tip for the four thickness surface zones are given in Table 1a. These yield parameters both increase with decreasing thickness as was expected. The final zone at a thickness of 3.175 mm has the rounded characteristic of a plane stress yield zone. The direction of maximum yielding, however, is still a fairly large angle relative to the crack line suggesting some influence of dilatation. Though for this problem (with a relatively small amount of plastic deformation present) the difference between the maximum radii is not large, the nature and extent of yielding ahead of the crack tip show a large dependence on the specimen thickness.

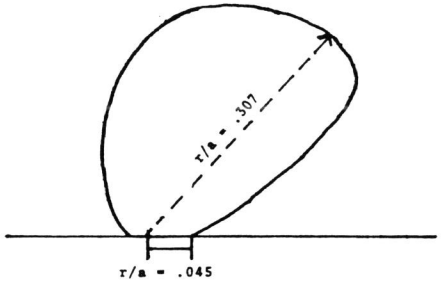

Fig. 3a. Surface yield zones for specimen with 2T = 2.54 cm.

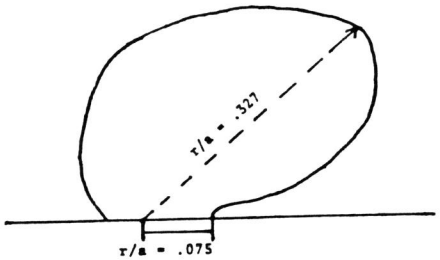

Fig. 3b. Surface yield zones for specimen with 2T = 1.27 cm.

Figure 4a is a plot of the von Mises stress contour corresponding to the material yield stress on the midplane of the 2.54 cmm thick specimen. The zone is typical of plane strain zones and is smaller than the surface zone for the same thickness specimen. The shape of the zone with a minimal extent of yielding ahead of the crack tip suggests high dilatation in that region. The midplane zone for the 1.27 cm thick specimen is shown in Fig. 4b. The zone is larger than that of the thicker specimen, however, there is still minimal yielding ahead of the tip. The angle of maximum yielding is more acute than in the thicker specimen. The stress state, however, would still be characterized by plane strain.

Figure 4c shows the midplane yield zone for the 6.35 mm thick specimen. The zone is considerably wider and more rounded than for the thicker specimens. It shows characteristics of both plane strain and plane stress zones suggesting a region of transition. Figure 4d is a plot of the midplane yield zone for the 3.175 mm thick specimen. The zone is basically a plane stress zone and is larger than for the thicker specimens. The maximum yield radii and radius of yielding ahead of the crack tip on the specimen midplanes are given in Table 1b. Both increase with decreasing thickness as was expected. In all cases, the midplane yield zones are smaller than the surface zones.

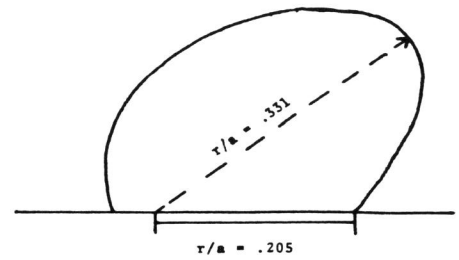

Fig. 3c. Surface yield zones for specimen with 2T = 6.35 mm.

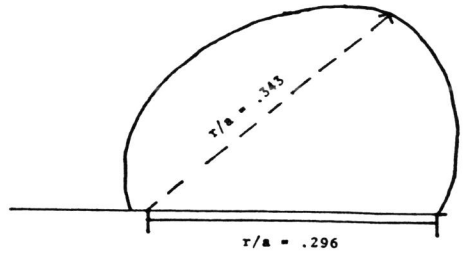

Fig. 3d. Surface yield zones for specimen with 2T = 3.175 mm.

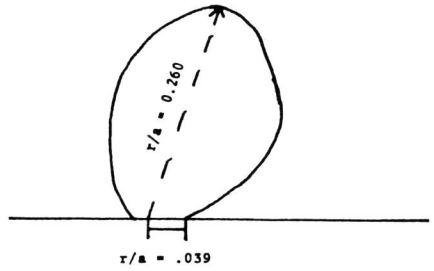

Fig. 4a. Midplane yield zones for specimen with 2T = 2.54 cm.

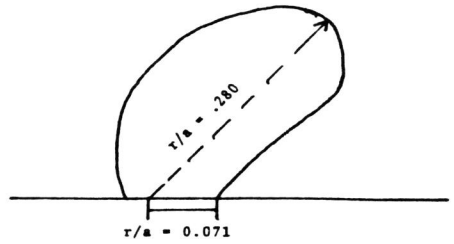

Fig. 4b. Midplane yield zones for specimen with 2T = 1.27 cm.

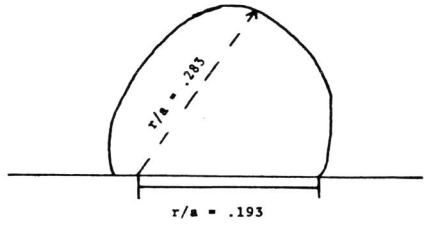

Fig. 4c. Midplane yield zones for specimen with 2T = 6.35 mm.

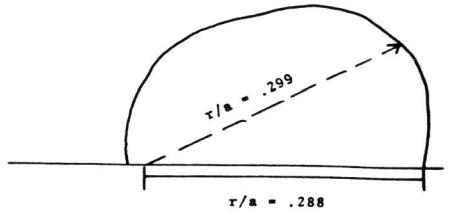

Fig. 4d. Midplane yield zones for specimen with 2T = 3.175 mm.

TABLE 1a Yield Radii as a function of Thickness for Surface Yield Zones.

Thickness	$r_{max/a}$	$r_{o/a}$
T = 2.54 cm	0.307	0.045
T = 1.27 cm	0.327	0.075
T = 6.35 mm	0.331	0.205
T = 3.175 mm	0.343	0.296

r_{max} → maximum yield radius

TABLE 1b Yield Radii as a Function of Thickness for Midplane Yield Zones.

Thickness	$r_{max/a}$	$r_{o/a}$
T = 2.54 cm	0.260	0.039
T = 1.27 cm	0.280	0.071
T = 6.35 mm	0.283	0.193
T = 3.175 mm	0.299	0.288

r_o → yield radius along crack line

CONCLUSIONS

The results of this study demonstrate the thickness dependence of the yield zones near a crack front on specimen thickness. It is shown that both the extent of plastic deformation and the dominance of deformation type (i.e., dilatation or distortion) are controlled by the thickness. The nature of the deformation is fundamental to the understanding of the incipient fracture processes. The delineation of the fundamental deformation response near a three-dimensional crack front is an imperative first step in the understanding and accurate prediction of ductile fracture processes.

To further the understanding of ductile fracture, it is necessary to compare theoretical and experimental deformation predictions local to the crack front. Only through such comparisons can an assessment be made of the accuracy and reliability of the numerical methods for plastic analysis. Toward this goal, it is proposed to measure the residual deformation on the surface of the specimen in the unloaded state. The theoretical study presented above demonstrates that the finite element predictions are qualitatively realistic and sensitive to specimen thickness. Comparison with experimental results will delineate the grid characteristics and hardening models which best model specific geometric and material applications. After successful "tuning" of the finite element model, a complete description of the stress and energy state in a cracked body can be predicted with confidence. Once fully three-dimensional stress fields are predicted, ductile failure theories can be tested and skeptically compared without the bias of unrealistic analytical approximations.

REFERENCES

Kachanov, L.M. (1971). Foundations of the Theory of Plasticity, North-Holland Publishing Co.

Moyer, Jr., E.T. and H. Liebowitz (1983). Plastic deformation and hardening characteristics in three-dimensional fracture specimens. Presented at the ICF International Symposium on Fracture Mechanics, Beijing, China, November 22-25.

Moyer, Jr., E.T. and H. Liebowitz (1983). Comparative study on three-dimensional crack tip modeling methodology. Presented at the International Conference on Application of Fracture Mechanics to Materials and Structures, Freiburg, Germany, June 20-24.

Zienkiewicz, O.C. (1977). The Finite Element Method, McGraw-Hill, New York.

ACKNOWLEDGMENT

This work was sponsored by the Office of Naval Research under Contract Number: N00014-75-C-0946.